PFC/RR-83-24

DOE/ET51013-95
UC-20 f

CALCULATION OF MOLYBDENUM SPUTTERING FROM THE LIMITER IN ALCATOR C

B. Lipschultz

Plasma Fusion Center
Massachusetts Institute of Technology
Cambridge, MA 02139

February 6, 1984

This work was supported by the U.S. Department of Energy Contract No. DE-AC02-78ET51013. Reproduction, translation, publication, use and disposal, in whole or in part by or for the United States government is permitted.

CALCULATION OF MOLYBDENUM SPUTTERING FROM THE LIMITER IN ALCATOR C

Abstract

A simple one-dimensional model for sputtering from the surface of a molybdenum limiter has been developed. Sources of sputtering included in this model are due to thermal ions and the subsequent self-sputtering that follows. The resultant molybdenum source rates match those calculated based on molybdenum line emission data from the main plasma coupled with an anomalous impurity diffusion coefficient. A review of the source rate dependence on plasma parameters is also included.

Introduction

Impurity radiation can have strong effects on tokamak plasmas, particulary high-Z impurities, which radiate from the plasma core. The power losses from such processes can cause the temperature profile to become centrally hollow and the plasma current to be disrupted. For the forseeable future high-Z materials will be utilized for internal hardware in tokamaks. It therefore behooves us to minimize the density of these impurities in the plasma core through reduction of the impurity confinement time in the main plasma and/or reduction of the impurity source rate at the plasma edge. The former is studied through the use of the laser-blowoff impurity injection technique [1]. The latter goal can be reached by either reducing the source generation at the material surface or by reducing its subsequent transport into the main plasma (by, for example, use of a divertor). The focus of this paper is the study of the impurity generation process at a material surface. The particular impurity involved in this study is molybdenum.

Molybdenum has been the limiter surface material in contact with the plasma for a majority of Alcator C discharges. Thorough characterizations of the effects of molybdenum impurities on the main plasma have appeared elsewhere [2-5]. The principal measurements of molybdenum radiation emission have been obtained from a 16-detector bolometer array and a flat-crystal grazing incidence spectrometer. Illustrative plots of results from these instruments are shown in figures 1 and 2 respectively. The relative brightness of Mo emission at 77Å, as a function of $\bar{n}_e$, is shown in figure 1. Measurements of molybdenum density in the main plasma vs. $\bar{n}_e$, as measured by the bolometer array, are shown in figure 2. Quite

rapid increases in molybdenum density in the main plasma are found as $\bar{n}_e$ is lowered. Although these measurements were obtained in discharges with a molybdenum limiter, the impurity behavior in graphite-limited in plasmas is qualitatively similar.

Impurity source modelling employing an anomalous diffusion coefficient in conjunction with the observations of intrinsic impurities (Figure 1), indicates the source of molybdenum also increases quite strongly with decreasing $\bar{n}_e$ [5]. The question arises -- what is the physical process that creates this source? If this question is answered, it may help us design limiters that reduce the impurity sources.

II. Possible Source Processes

There are two mechanisms by which high-Z impurities can be removed from a surface [6]: evaporation and physical sputtering. Lower Z materials can be removed through these and other processes as well. The study of molybdenum is more attractive than, for example, carbon because the number of possible removal processes are fewer. For a thorough review of impurity source generation mechanisms, see McCracken [6].

Evaporation involves a local heating of the surface. This could occur through thermal plasma flow to the limiter or through more exotic processes such as unipolar arcs and runaway electrons which create local 'hot' spots.

Physical sputtering involves a momentum transfer process. An incident particle imparts energy $E > E_{binding}$ to a surface atom in a direction out of the surface. The incident particle must be of proper mass as well

as energy to efficiently transfer momentum. Typically, the sputtering coefficients peak at $m_1 = m_2$ where the subscript refers to incident and sputtered particles. Physical sputtering obviously involves multiple collisions since the incident and sputtered particles travel in opposite directions.

As a consequence of the dependencies detailed above, the sputtering coefficient can be described as follows [7]:

$$S(E) = \frac{C}{E_B} Z_1^{0.75} (Z_2 - 1.8)^2 \left(\frac{M_1 - .8}{M_2}\right)^{1.5} \times \frac{(E - E_{th})}{(E - E_{th} + 50\, Z_1^{0.75} Z_2)^2} \quad (1)$$

C = 2000 for incident hydrogen

= 400 for all other particles

E_B = binding energy of material

E_{th} = threshold energy for sputtering

$$= E_B \frac{(4M_1 + M_2)^2}{4M_1M_2} \quad (2)$$

Further characterization of the source behavior would be useful for determining whether evaporation or physical sputtering is the dominant process. The dependence of the source rate on $\bar{n}_e$, with a molybdenum limiter installed in the tokamak was discussed in the introduction to this paper. The $\bar{n}_e$ dependence is qualitatively similar with a graphite limiter but the magnitude of the rate is much reduced. This indicates

that the primary source for molybdenum is the limiter for molybdenum limiter discharges. It is also true that molybdenum is plated on the vacuum vessel walls during these discharges so that when the molybenum limiter is removed, the primary site becomes other vessel components. More important, the impurity generation process appears to remain the same due to similarities in the $\bar{n}_e$ dependences.

Another parameter upon which the molybdenum source depends, is the background gas mass. As the mass of the background gas is increased, so does the molybdenum source rate. This seems to imply that physical sputtering is the dominant process but other possibilities need to be discussed.

Experimental measurements indicate the source rate is constant on the discharge time scale. This disqualifies runaway electron and unipolar arcs which tend to cause time dependent molybdenum influxes. Such 'bursts', in fact, are seen in the experiment as 'natural' injections. The only evaporation process left is thermal loading. Thermocouple measurements show that the power to the limiter increases roughly proportional to $\bar{n}_e$ [8] (see Figure 3). This would produce a source rate dependence opposite to that which is observed.

Physical sputtering remains to be discussed. Charge-exchange neutrals from the main plasma or charged ions flowing through the edge will cause surface sputtering. Charge exchange flux ($E > 1$ keV) to the wall increases as the plasma density is lowered [9]. Although this $\bar{n}_e$ dependence is what we seek, the source dependence on background gas mass is not. As stated above, the molybdenum source rate increases with the mass of the background gas. But the flux of charge exchange neutrals out of a

helium plasma is much lower than for a hydrogenic plasma.

Physical sputtering, due to the flow of ions in the edge, does match the mass dependence we seek . The decrease in thermal flux to the limiter with with decreasing $\bar{n}_e$ has been discussed. The $\bar{n}_e$ dependence of the ion sputtering, due to this thermal plasma, has the opposite trend: The flux to the limiter is approximately equal to $n_{edge}\ C_s \propto n_{edge} \sqrt{T_{edge}}$. If $n_{edge} \times T_{edge}$ is a constant function of $\bar{n}_e$, then the flux ($\Gamma_{thermal}$) $\propto n_{edge}^{1/2} \sim (\bar{n}_e)^{1/2}$. We must multiply this flux by a sputtering coefficient, S(T), to obtain the total sputtered flux ($\Gamma_{sputtered}$)

$$\Gamma_{sputtered} = \Gamma_{thermal} \times S(T)$$

As can be seen from Figure 4, S(T) has a much stronger dependence than $T_{edge}^{1/2}$, above a threshold energy.

$$\Gamma_{sputtered} \sim T_{edge}^{-1/2} \times e^{T_{edge}}$$

$$\sim e^{T_{edge}}$$

This is the density (temperature) dependence we have been searching for, given that Langmuir probe measurements show T_{edge} rises as $\bar{n}_e$ decreases [10].

Plasma Sheath Models

Electrons are much more mobile than ions by the factor $\sqrt{m_i/m_e}$. Examining a field line in the edge, electrons are found to be lost to the wall much faster than ions. These field lines become positively charged with respect to the wall. The resulting potential, confined to

several debye lengths in distance from the wall, adjusts itself until the ion and electron currents to the wall are equal. This is called the plasma sheath. Only electrons with energy $1/2\ mv_s^2 > e\phi_{sheath}$ will reach the wall. If the ion and electron currents are equal at a point very far away from the wall ($x = \infty$) along the field line then

$$n_e \int_{v_s}^{\infty} v_x g_e(v_x) dv_x = n_e \int_{o}^{\infty} v_x g_i(v_x) dv_x \tag{2}$$

To obtain $g_{e,i}(v_x)$, the electron (ion) v_x distribution function, we must integrate the corresponding general distribution function over v_y & v_z. Rewriting (2) after this integration, and assuming $T_e = T_i = T$, we find

$$m_e^{1/2} \int_{v_s}^{\infty} v_x e^{-m_e v_x^2/2kT} dv_x = m_i^{1/2} \int_{o}^{\infty} v_x e^{-m_i v_x^2/2kT} dv_x \tag{3}$$

Solving for v_s and, therefore, ϕ_{sheath},

$$e\phi_{sheath} = \frac{kT}{2} \ln \frac{m_i}{m_e} \tag{4}$$

For H_2 this value is ~ 3.8 kT.

More importantly, the average energy carried by electrons in the x direction can be determined

$$\langle W_{xe} \rangle = \frac{\int_{v_s}^{\infty} \frac{1}{2} mv_x^2 \, v_x e^{-mv_x^2/2kT} dv_x}{\int_{v_s}^{\infty} v_x e^{-mv_x^2/2kT} dv_x} \tag{5}$$

$$= e\phi_s + kT$$

$$\Longrightarrow \quad \langle W_e \rangle = e\phi_s + 2kT \tag{6}$$

The similar calculation for ions yields

$$\langle W_i \rangle = 2\ kT$$

$$\Longrightarrow \quad \langle W_{TOT} \rangle = \langle W_i \rangle + \langle W_e \rangle = e\phi_s + 4\ kT \tag{7}$$

The above calculations give the energy carried by ions and electrons up to the sheath. In traveling through the sheath, the energy $e\phi_s$ is transferred from electrons to ions. The total heat flow to the wall, Q_{TOT}, is:

$$Q_{TOT} = \Gamma \langle W_{TOT} \rangle$$

$$= \frac{n\bar{v}}{4} \langle W_{TOT} \rangle$$

$$= n\sqrt{\frac{kT}{2\pi M_i}} \times (e\phi_s + 4kT) \tag{8}$$

Of primary interest is the ion energy and flux to the wall:

$$\langle W_i \rangle_{wall} = e\phi_s + 2kT \tag{9}$$

$$\Gamma_{ion} = n\sqrt{\frac{kT}{2\pi M_i}} \tag{10}$$

The purpose of this exercise has been to give a physical understanding of the plasma sheath. Many processes, however, have been ignored: Energy losses (gains) or physical mechanisms that could preferentially drive particles (e.g. rf) along the length of the field line.

Recycling near the wall, or other particle sources, can cause local increases in $e\phi$. There can be reflection of particles and/or secondary electron emission at the wall. The wall itself has some work function which must enter into the calculation. All of these processes should be included.

Further physical insight into the sheath can be obtained by examining the solution to Poissons equation at the sheath [11]. One can solve for the velocity $(u(x))$ within the sheath using energy and momentum conservation:

$$e\phi(x) + \frac{1}{2} m_i u^2(x) = \frac{1}{2} m_i u_o^2 \tag{11}$$

$$n(x)u(x) = n_o u_o \tag{12}$$

$$\Longrightarrow \quad n_i(x) = n_o \left(1 - \frac{2e\phi(x)}{M_i u_o^2}\right)^{-1/2} \tag{13}$$

The subscript o refers to values of those variables at the sheath edge. Substituting (13) into Poisson's equation, one finds that there are solutions only if the ion velocity at the sheath edge, u_o, is greater than the sound speed. This is called the Bohm Sheath Criterion. The implication is that there is some long range electric field which accelerates ions and decelerates electrons. The magnitude of this 'presheath' potential is $1/2\ mv_s^2 \sim kT/2$. This treatment ignores no less than the integral treatment above. There are a host of more rigorous calculations to be found in the literature. For a thorough listing see reference [12].

The form for ion flux and energy through the sheath, developed by Emmert [12], has been used for this exercise. Essentially, the Emmert model is a fully kinetic treatment through the sheath. Particle sources are allowed outside the sheath. The flux and energy per ion hitting the wall are:

$$\Gamma = \beta \sqrt{\frac{kT}{2\pi M_i}} \tag{14}$$

$$\langle W_i \rangle = 2\mu kT + e(\phi_{sheath} - \phi_{wall}) \tag{15}$$

For the case of $T_e = T_i$, and $Z = 1$, we find $\beta = 2.2$, $\mu = 1.2$ and $e(\phi_{sheath} - \phi_{wall}) = 2.5kT$. The values for Γ and $\langle W_i \rangle$ are certainly different from those of the simpler calculations above. Emmert explains the factor β as being due to the difference between the distribution function he finds (half space maxwellian @ $x = \infty$), and a full-space maxwellian.

Numerical Model

The computer code developed for this application is one-dimensional along a minor radius in the scrape-off layer. Langmuir probe measurements of density and temperature in the plasma edge are used as input [10]. An analytic form [13] is fitted to this data for ease of evaluating the flux and energy of ions to the limiter. A numerical subroutine DSPUT [7] is used to finish the calculation by evaluating the sputtering coefficient.

The analytic forms used for the density and temperature profiles are

$$n_e(r) = n_e\,(r = a)\, \exp -(r - a)/\lambda_n \tag{16}$$

$$T_e(r) = T_e\ (r = a)\ \exp -(r - a)/\lambda_T \qquad (17)$$

so that four parameters specify both profiles. Plots of these parameters are shown in Figures 5 and 6. The probe measurements are for D_2 working gas . A complete set of $(n_e(r),\ T_e(r))$ measurements for all plasma $\bar{n}_e$ is not available. Interpolation and extrapolation of the data is performed when needed utilizing limiter thermocouple measurements of thermal loading as a check. (Figure 3).

Results

The results of this calculation are given by line (b) in Figure 7. This should be compared with line (a), the impurity source as determined from observations of intrinsic impurities (figure 1) , in conjunction with an empirically derived anomalous impurity diffusion model [5]. Both lines (a) and (b) are determined from D_2 discharges utilizing a 16.5 cm radius molybdenum limiter. The uncertainty limits shown for the points of line (b) reflect the range in experimental values shown in Figures 3, 5 and 6. There is a possible factor of 2 uncertainty in line (a) due to possible variations in source location. The conclusion is that these calculations are not in agreement.

The obvious physical process that might account for this disagreement is self-sputtering. The molybdenum sputtered by the D_2 thermal ions is ionized and returns to the limiter. These ions, because of their mass and charge, can have rather large sputtering coefficients (see Figure 4). To properly include self-sputtering, a two-dimensional impurity transport model for the edge would have to be developed. Such a calculation is beyond the scope of this study.

A crude model for the sputtered molybdenum behavior has therefore been implemented. Fifteen percent of the sputtered molybdenum is assumed to enter the plasma with 85% remaining in the edge. Furthermore, the molybdenum that enters the plasma returns to the edge with $\langle q/e \rangle = 6$. The molybdenum that remains in the edge plasma is ionized to a charge state which is a function of T_{edge}. This charge state dependence on T_{edge} is evaluated using the data of reference 14. In steady state, all of this ionized molybdenum returns to the limiter and sputters more molybdenum. The final result of this repetitive process is an infinite series;

$$\Gamma_{sput} = \Gamma_{\substack{thermal \\ sput}} \times \left(1 + \sum_{i=1}^{\infty} (S_{eff})^i\right)$$

$$= \Gamma_{\substack{thermal \\ sput}} / (1 - S_{eff}) \qquad (18)$$

where Γ_{sput} is the total number of sputtered molybdenum atoms including self sputtering. $\Gamma_{\substack{thermal \\ sput}}$ is the sputtered molybdenum flux due to thermal ions. The effective sputtering coefficent, S_{eff}, is described by

$$S_{eff} = .15 \times S(T_{edge}, Z = 6) + .85 \times S(T_{edge}, Z_{edge}) \qquad (19)$$

reflecting the contributions of sputtering coefficients determined by molybdenum atoms ionized in the main and edge plasmas respectively.

Inclusion of self-sputtering in the numerical model yields line (c) in Figure 6. This result is much closer to the impurity transport calculation (line a). The difference lies within the uncertainties of the models. In fact, if the ions were allowed to be hotter than the electrons, the results would most likely match.

Conclusions

A very simple one dimensional model of sputtering has been developed. Results agree with separate calculations of the molybdenum source rate based only on the molybdenum density in the main plasma and an anomalous impurity diffusion coefficient. This edge sputtering model was not applied to constituent gasses other than D_2 due to lack of probe measurements which are used as input. However, the scaling with the mass of the background gas agrees with central plasma measurements.

The question still remains: What is the molybdenum source without a molybdenum limiter present? One possible explanation is that two processes are involved: physical sputtering by charge exchange neutrals to provide a background level and self sputtering as well. It is fairly simple to calculate the charge exchange flux spectrum of neutrals from the main plasma using the FRANTIC code [15]. The subroutine DSPUT can then be used to evaluate the sputtered flux assuming 10% of the wall is covered with molybdenum. Line (d) in Figure 7 indicates the result. Self sputtering by molydenum is not included in this calculation. The uncertainty range represents the variability of specifying the edge neutral density dependence on $\bar{n}_e$. Further experimental work would be quite useful in understanding this question.

Acknowledgements

The author thanks J. Brooks of Argonne National Lab for the use of DSPUT and C. Fiore of M.I.T. for help with FRANTIC. Discussions with J. Rice, J. Terry, B. LaBombard, S. Wolfe, and M. Pickrell were informative and encouraging.

Figure Captions

Figure 1: Brightness at 77Å (M_o^{25+}) as a function of line average electron density, $\bar{n}_e$ at constant current, with a 10 cm molybdenum limiter.

Figure 2: Central molybdenum density determined from bolometer measurements of radiated power profiles.

Figure 3: Energy deposited on a 16.5 cm molybdenum limiter during a discharge vs. $\bar{n}_e$. Values of power loading are calculated assuming energy is deposited over a fixed shot length.

Figure 4: Sputtering coefficient for; deuterium ions incident on molybdenum (----); and molybdenum ions incident on molybdenum (- - -).

Figure 5: Parameters describing the density profile vs. $\bar{n}^e$; n_{eo}, λ_n.

Figure 6: Parameters describing the temperatures profile vs. $\bar{n}_e$; T_{eo}, λ_T.

Figure 7: Calculated molybdenum influx as a function of $\bar{n}_e$. Line (a) is from impurity transport modeling employing the data of Figure 1. Line (b) is the prediction assuming molybdenum is sputtered by thermal ions only. Line (c) is the results shown by line (b) but with molybdenum self sputtering included. Line (d) is the source due to neutral sputtering of molybdenum from a wall 10% covered by molybdenum.

References

[1] E. S. Marmar, J. E. Rice, J. L. Terry, & F. H. Seguin, Nuclear Fusion, 22, 1567 (1982).

[2] R. R. Parker, M. M. Pickrell, B. Lipschultz, Bull. Amer. Phys. Soc., 27, 937 (1982).

[3] M. M. Pickrell, "The Role of Radiation on the Power Balance of the Alcator C Tokamak" M.I.T. Plasma Fusion Center Report PFC/RR-82-30.

[4] J. E. Rice, E. S. Marmar, K. J. Pinto, "Application of the Emperical Anomalous Impurity Diffusion Model to Interpret Observations of Molybdenum and Chlorine Radiation From Alcator C", Bull. Amer. Phys. Soc., 27, 937 (1982)

[5] J. E. Rice, E. S. Marmar, B. Lipschultz, J. L. Terry, Submitted to Nuclear Fusion.

[6] G. M. McCracken, B. E. Stott, Nucl. Fusion, 19, 889 (1979).

[7] D. L. Smith, J. N. Brooks, D. E. Post, D. B. Heifetz, Proceedings of the 9th Sympsium of Engineering Problems of Fusion Research, Oct. 1981, Chicago, USA.

[8] B. Lipschultz, et al., Bull. Amer. Phys. Soc., 26, 975 (1981).

[9] C. L. Fiore, Private communication.

[10] B. LaBombard, B. Lipschultz, M. M. Pickrell, Y. Takase, Bull. Amer. Phys. Soc., 27, 1037 (1982).

[11] F. F. Chen, Introduction to Plasma Physics, Plerion Press, New York, (1974) p. 245-6.

[12] G. A. Emmert, et al., Phys. of Fluids, 23, 803 (1980).

[13] K. Uehara, et al., Plasma Physics, 21, 89 (1979)

[14] TFR Group, Plasma Physics 19, 587(1977)

[15] H. H. Towner, R. J. Goldston, D. C. McCune, and S. Tamor, Bull. Amer. Phys. Soc., 26, 857 (1981).

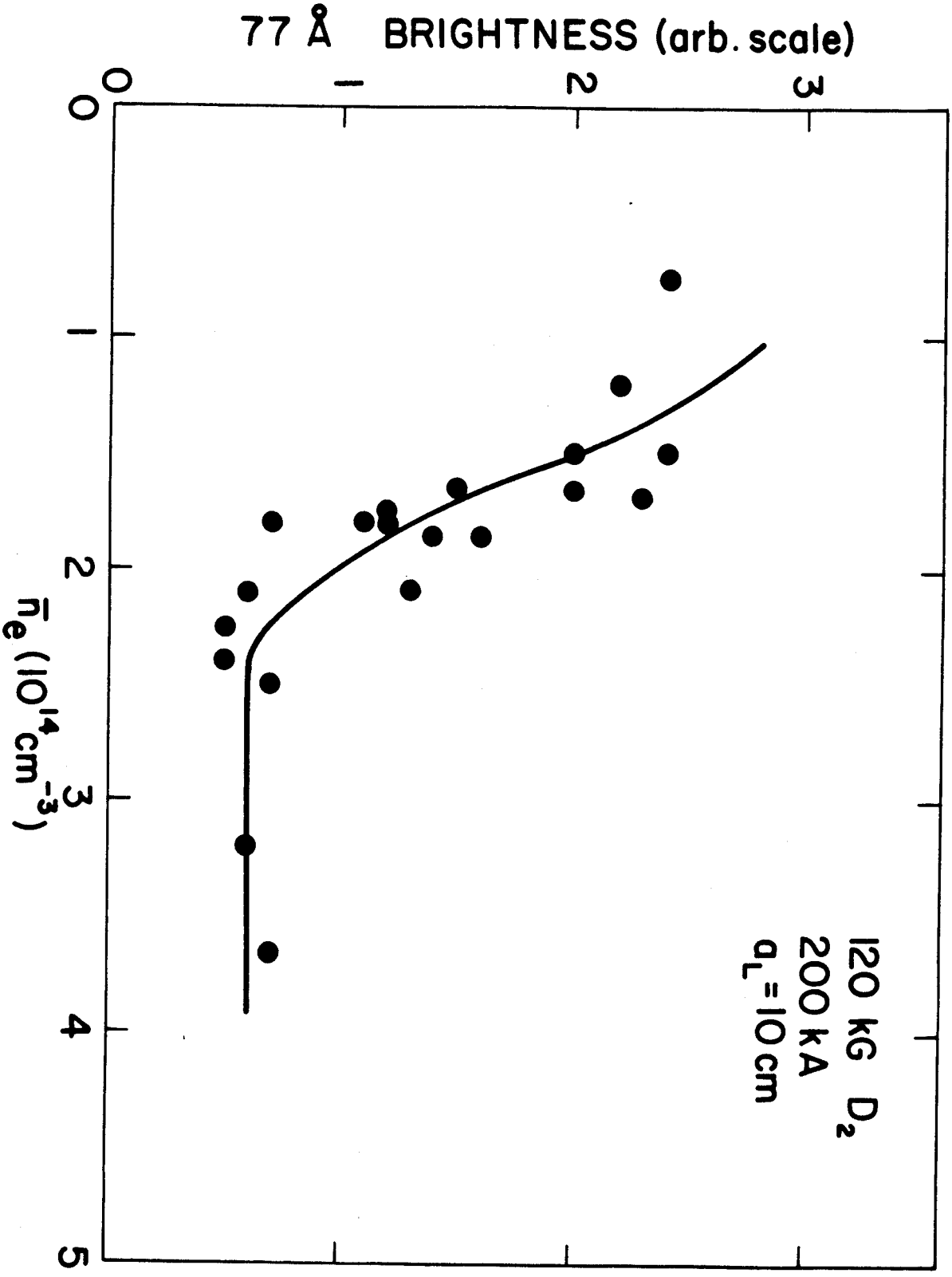

PFC-8159

FIGURE 1

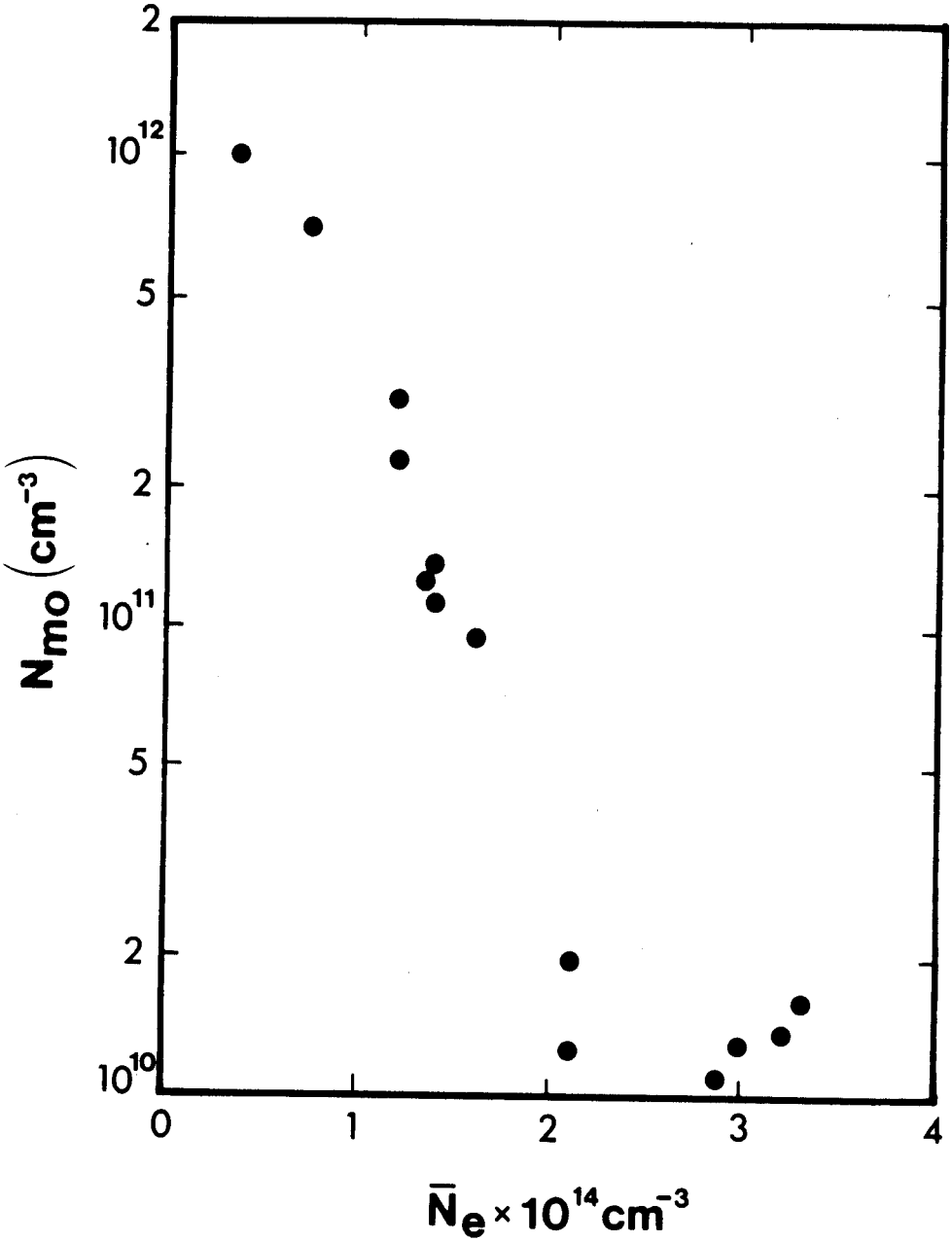

FIGURE 2

8969

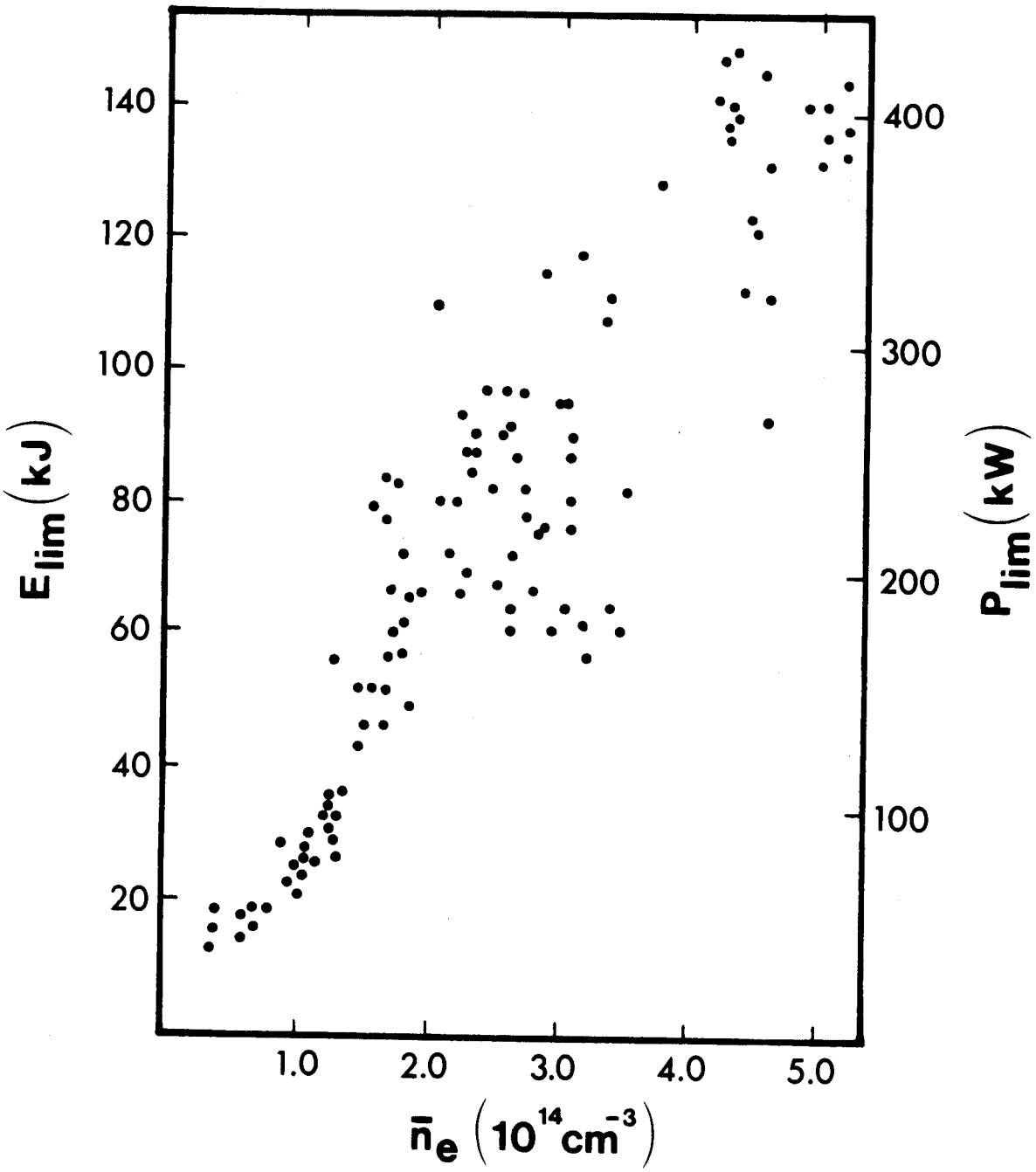
140
120
100
80
60
40
20
E_{lim} (kJ)
400
300
200
100
P_{lim} (kW)
1.0
2.0
3.0
4.0
5.0
$\bar{n}_e$ $(10^{14} cm^{-3})$

FIGURE 3

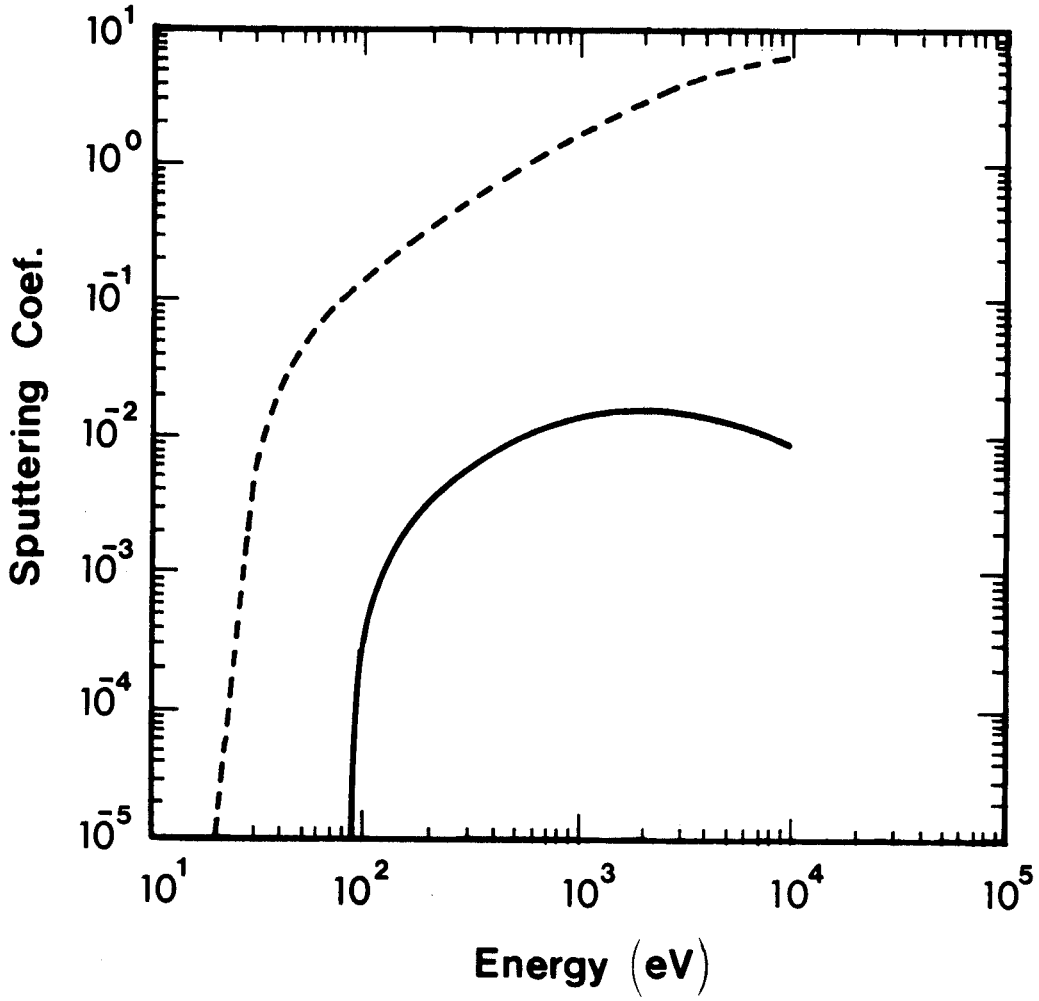
Sputtering Coef.
10^{1}
10^{0}
10^{-1}
10^{-2}
10^{-3}
10^{-4}
10^{-5}
10^{1}
10^{2}
10^{3}
10^{4}
10^{5}
Energy (eV)

FIGURE 4

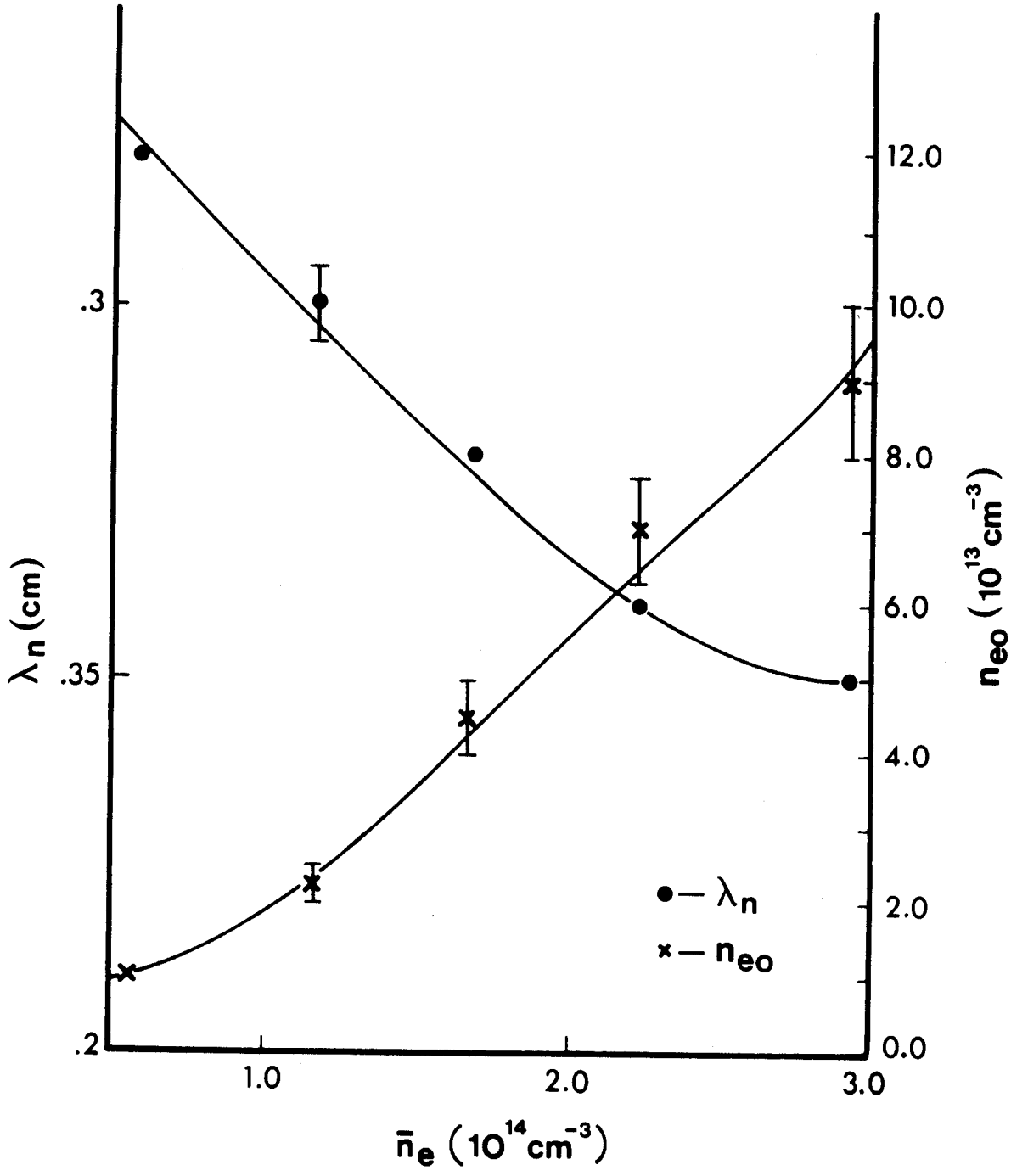

8467

FIGURE 5

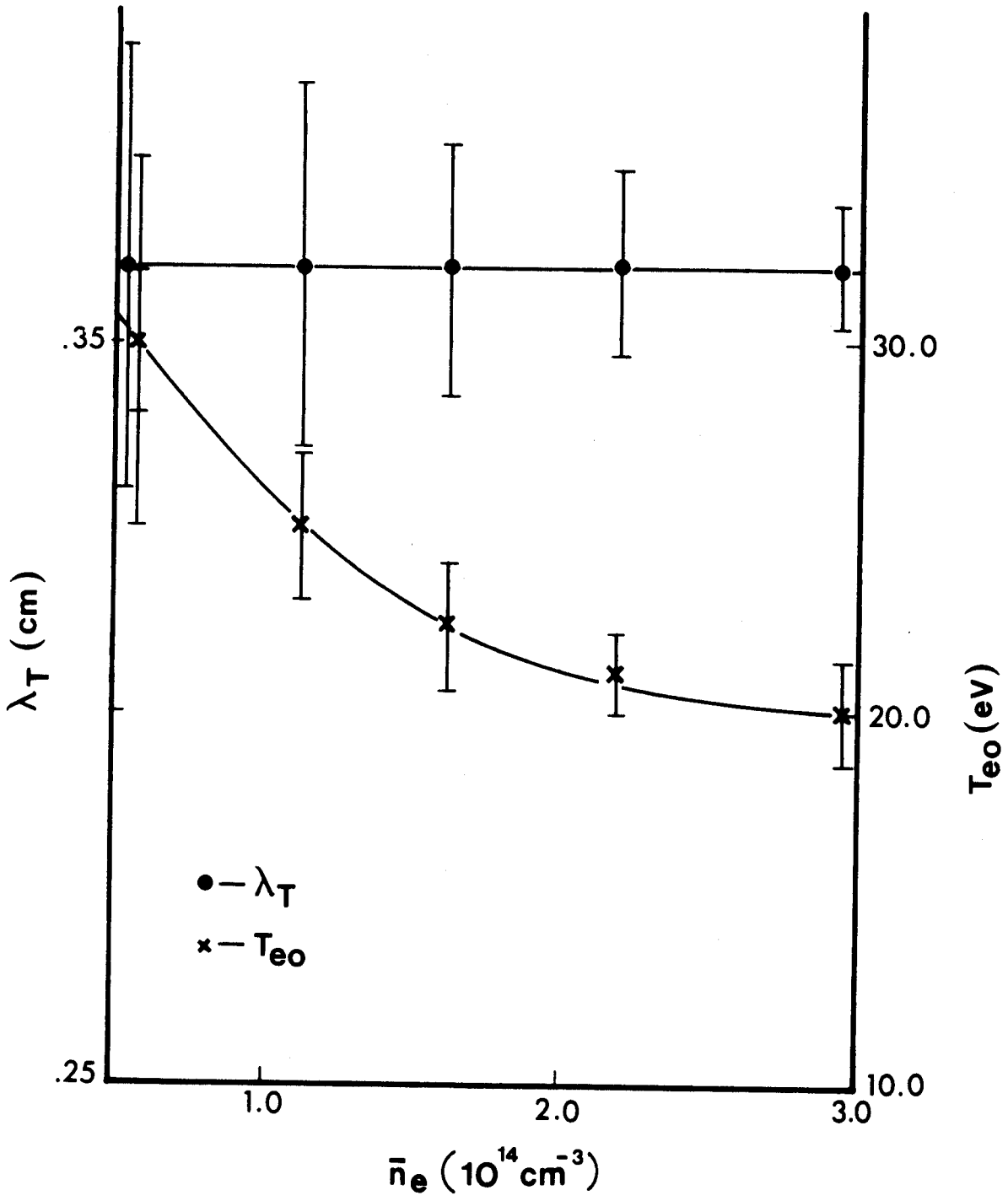

FIGURE 6

8466

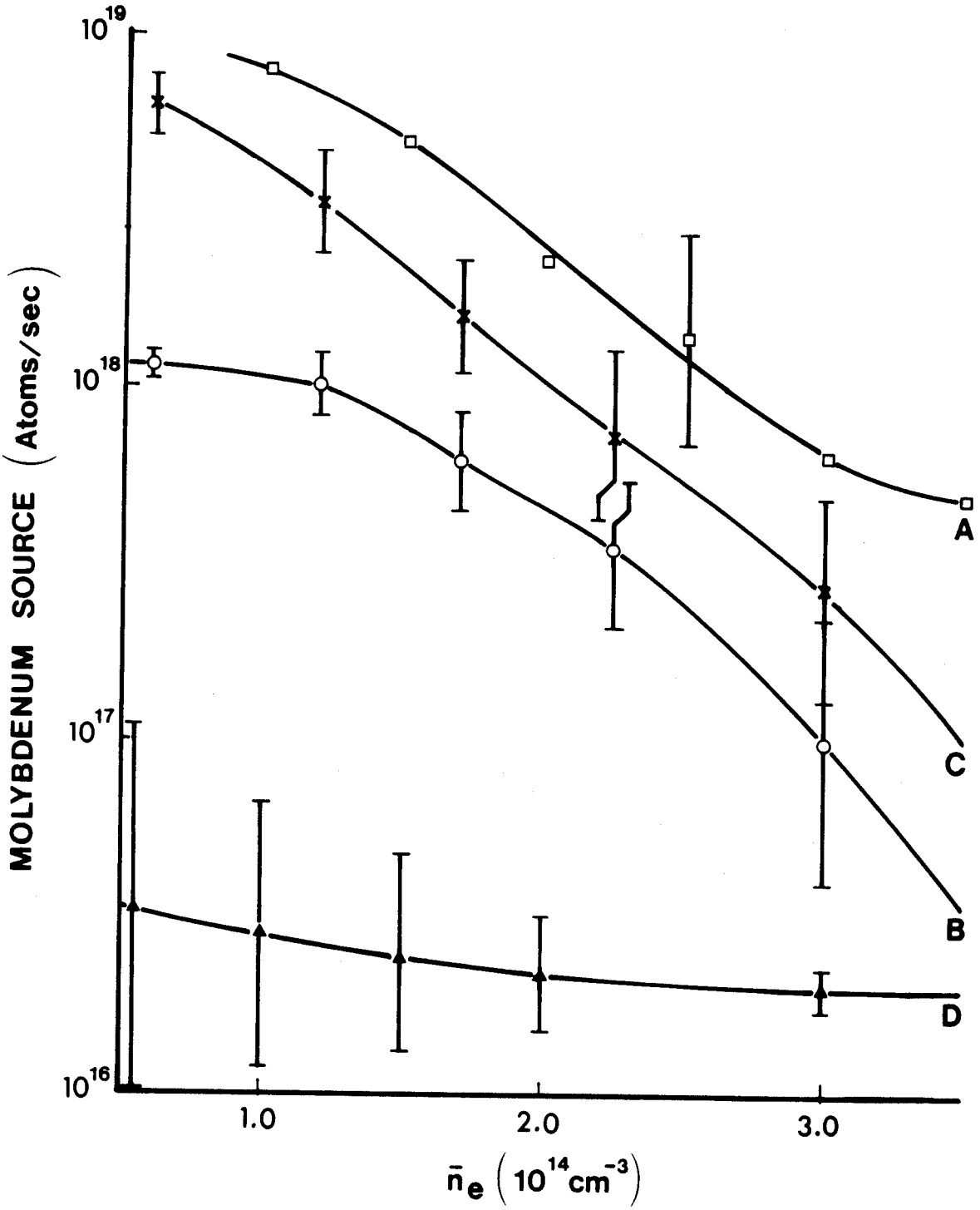

FIGURE 7

0446